

Advanced Finite Element Method for Nano-Resonators

Lin Zschiedrich^{a,b}, Sven Burger^{a,b}, Benjamin Kettner^a, and Frank Schmidt^{a,b}

^a Zuse Institute Berlin (ZIB), Takustraße 7, D-14195 Berlin, Germany

^b JCMwave GmbH, Haarer Straße 14a, D-85640 Putzbrunn, Germany

Copyright 2006 Society of Photo-Optical Instrumentation Engineers.

This paper will be published in Proc. SPIE **6115** (2006), (*Physics and Simulation of Optoelectronic Devices XIV*). and is made available as an electronic preprint with permission of SPIE. One print or electronic copy may be made for personal use only. Systematic or multiple reproduction, distribution to multiple locations via electronic or other means, duplication of any material in this paper for a fee or for commercial purposes, or modification of the content of the paper are prohibited.

ABSTRACT

Miniaturized optical resonators with spatial dimensions of the order of the wavelength of the trapped light offer prospects for a variety of new applications like quantum processing or construction of meta-materials. Light propagation in these structures is modelled by Maxwell's equations. For a deeper numerical analysis one may compute the scattered field when the structure is illuminated or one may compute the resonances of the structure. We therefore address in this paper the electromagnetic scattering problem as well as the computation of resonances in an open system. For the simulation efficient and reliable numerical methods are required which cope with the infinite domain. We use transparent boundary conditions based on the Perfectly Matched Layer Method (PML) combined with a novel adaptive strategy to determine optimal discretization parameters like the thickness of the sponge layer or the mesh width. Further a novel iterative solver for time-harmonic Maxwell's equations is presented.

Keywords: Nano-Optics, Meta-Materials, Resonances, Scattering, Finite-Element-Method, PML

1. INTRODUCTION

With the advances in nanostructure physics it has become possible to construct light resonators on a lengthscale equal to or even smaller than optical wavelengths.^{1,2} These nanostructures are large on the atomic scale, therefore they can be of complex geometry and they may possess properties not occurring in nature, like an effective negative index of refraction³ which allows in principle to overcome limits in the resolution of optical imaging systems.⁴

The numerical simulation of light fields in such structures is a field of ongoing research. In this paper we report on finite element methods for the efficient computation of resonances and light propagation in arbitrarily shaped structures embedded in simply structured, infinite domains. Section 2 introduces our concept of discretizing exterior infinite domains. Section 3 recapitulates a formulation of Maxwell's equations for time-harmonic scattering problems. Section 4 introduces an adaptive method for the efficient discretization of the exterior domain based on the PML method introduced by Berenger.⁵ Section 5 shows the weak formulation of Maxwell's equations which is needed for the finite-element method. In Section 6 we shortly introduce a new preconditioner for the numerical solution of indefinite time-harmonic Maxwell's equations. Finally, in Sections 8 and 9 we test our algorithms on nano-optical real world problems: the computation of resonances and scattering in arrays of split-ring resonators and in isolated pyramidal nano-resonators.

Further author information: (Send correspondence to Lin Zschiedrich)

E-mail: zschiedrich@zib.de

URL: <http://www.zib.de/nano-optics/>

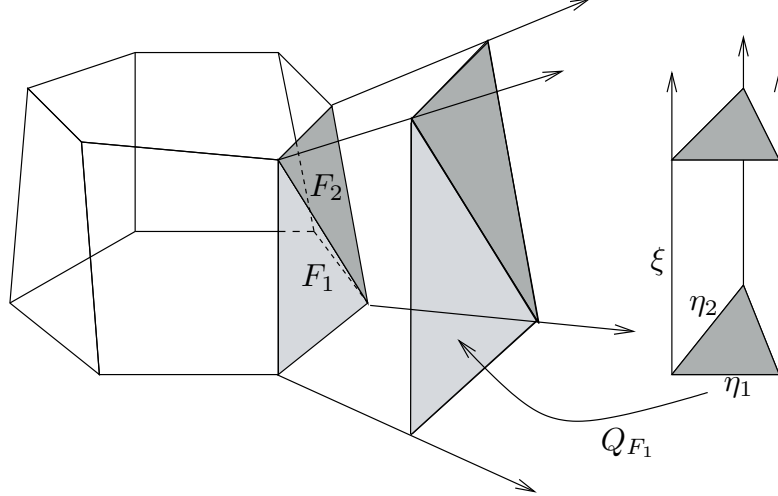


Figure 1. Infinite domain. The interior domain (left) may contain nearby arbitrarily shaped objects. The exterior domain consists of prisms attached to triangular boundary faces of the interior domain. Each prism is the image of the unit prism (right) under a bilinear mapping such that the triangles with $\xi = \text{const}$ are mapped to parallel triangles. For each infinite prism we assume constant material parameters.

2. GEOMETRIC CONFIGURATION

In this section we explain how to specify an infinite geometry such that it fits well to the finite element method (FEM). The geometry is split into a bounded interior domain Ω_{int} and an unbounded exterior domain Ω_{ext} . The interior domain may contain nearby arbitrary shaped structures such as spheres or thin layers. The geometry in the exterior domain is more restricted. However, the construction we propose is general enough to deal with typical geometries of optical devices.

We assume that the boundary Γ of the interior domain consists of triangles. A boundary triangle $F \subset \Gamma$ is called *transparent* if $F \subset \partial\Omega_{\text{ext}}$. Further we introduce the unit prism $P_u = \{(\eta_1, \eta_2, \xi) \in \mathbf{R}^3 : \eta_1, \eta_2, \xi \geq 0, \eta_1 + \eta_2 \leq 1\}$. An exterior domain is admissible if the following conditions are satisfied. For each boundary triangle F there exists a bilinear one-to-one mapping Q_F from the unit prism into the exterior domain Ω_{ext} such that each triangle $T_\rho = \{(\eta_1, \eta_2, \xi) \in P_u : \xi = \rho\}$ is mapped onto a triangle parallel to the face and such that the bottom triangle of the unit patch is mapped onto the corresponding face, $Q_F T_0 = F$, cf. Figure 1. The image of Q_F is denoted by P_F . Hence we attach the infinite prism P_F to the transparent face F . It must hold true that $\Omega_{\text{ext}} = \cup_F P_F$. Further we demand the following matching condition. If $Q_F(\eta_1, \eta_2, 0) = Q_{F'}(\eta'_1, \eta'_2, 0)$, that is F and F' have a common point, then $Q_F(\eta_1, \eta_2, \xi) = Q_{F'}(\eta'_1, \eta'_2, \xi)$ for all $\xi \in \mathbf{R}_+$.

The surface $S_\rho = \cup_F Q_F T_\rho$ looks like a “stretched” transparent boundary of the interior domain. Hence the coordinate ξ is chosen consistently for all prism such that it serves as a generalized distance variable. This is essential for the pole condition concept developed by Frank Schmidt.⁶ For later purposes we introduce the truncated unit prism $P_\rho = \{(\eta_1, \eta_2, \xi) \in \mathbf{R}^3 : \eta_1, \eta_2 \geq 0, \eta_1 + \eta_2 \leq 1, 0 \leq \xi \leq \rho\}$ and the truncated exterior domain $\Omega_\rho = \cup_F Q_F P_\rho$.

If there exist triangles on Γ which are not transparent, then either boundary conditions must be imposed on them, or they must be identified with other periodic triangles (e.g., when Ω is a cell of a periodic structure). However for simplicity we assume that $\Omega_{\text{int}} \cup \Omega_{\text{ext}} = \mathbf{R}^3$ in rest of the paper.

3. SCATTERING PROBLEMS

Monochromatic light propagation in an optical material is modelled by the time-harmonic Maxwell’s equations

$$\text{curl } \mu^{-1}(\vec{x}) \text{ curl } \mathbf{E}(\vec{x}) - \omega^2 \varepsilon(\vec{x}) \mathbf{E}(\vec{x}) = 0, \quad (1a)$$

$$\text{div } \varepsilon(\vec{x}) \mathbf{E}(\vec{x}) = 0, \quad (1b)$$

which may be derived from Maxwell's equations when assuming a time dependency of the electric field as $\mathbf{E}(\vec{x}, t) = \mathbf{E}(\vec{x}) \exp(-i\omega t)$ with angular frequency ω . The dielectric tensor ε and the permeability tensor μ are L^∞ functions of the spatial variable $\vec{x} = (x_1, x_2, x_3)$. In addition we assume that the tensors ε and μ are constant on each infinite prism as defined in the previous section. For simplicity assume that the dielectric and the permeability tensors are isotropic so they may be treated as scalar valued functions. Recall that any solution to (1a) with $\omega \neq 0$ also meets the divergence condition (1b).

A scattering problem may be defined as follows: Given an incoming electric field \mathbf{E}_{inc} satisfying the time-harmonic Maxwell's equations (1) for a fixed angular frequency ω in the exterior domain, compute the total electric field \mathbf{E} satisfying (1) in $\Omega_{\text{int}} \cup \Omega_{\text{ext}}$, such that the scattered field $\mathbf{E}_{\text{sc}} = \mathbf{E} - \mathbf{E}_{\text{inc}}$ defined on Ω_{ext} is *outward radiating*. For a precise definition of when a field is outward radiating we refer to Schmidt.⁶ Hence the scattering problem splits into an interior subproblem for $\mathbf{E}_{\text{int}} = \mathbf{E}|_{\Omega_{\text{int}}}$ on Ω_{int}

$$\text{curl } \mu^{-1} \text{curl } \mathbf{E}_{\text{int}} - \omega^2 \varepsilon \mathbf{E}_{\text{int}} = 0,$$

and an exterior subproblem on Ω_{ext}

$$\text{curl } \mu^{-1} \text{curl } \mathbf{E}_{\text{sc}} - \omega^2 \varepsilon \mathbf{E}_{\text{sc}} = 0.$$

These subproblems are coupled by the following matching conditions:

$$\mathbf{E}_{\text{int}} \times \vec{n} = (\mathbf{E}_{\text{inc}} + \mathbf{E}_{\text{sc}}) \times \vec{n} \quad (2)$$

$$\mu^{-1} \text{curl } \mathbf{E}_{\text{int}} \times \vec{n} = \mu^{-1} \text{curl } (\mathbf{E}_{\text{inc}} + \mathbf{E}_{\text{sc}}) \times \vec{n} \quad (3)$$

on the boundary $\partial\Omega_{\text{int}}$.

4. ADAPTIVE PML METHOD

The perfectly matched layer method was originally introduced by Berenger in 1994.⁵ The idea is to discretize a complex continued field in the exterior domain which decays exponentially fast with growing distance to the interior-exterior domain coupling boundary. This way a truncation of the exterior domain only results in small artificial reflections. The exponential convergence of the method with growing thickness of the sponge layer was proven for homogeneous exterior domains by Lassas and Somersalo.^{7,8} An alternative proof with a generalization to a certain type of inhomogeneous exterior domain is given by Hohage et al.⁹ Nevertheless as shown in our paper¹⁰ the PML method intrinsically fails for certain types of exterior domains such as layered media. This is due to a possible total reflection at material interfaces. In this case there exists a *critical* angle of incidence for which the resulting field in the exterior domain is neither propagating nor evanescent. Here we show that it is possible to overcome these difficulties when using an adaptive method for the discretization of the exterior domain problem. We assume the following expansion of the scattered field in the exterior domain

$$\mathbf{E}_{\text{sc}}(\eta_1, \eta_2, \xi) \sim \int \mathbf{c}(\eta_1, \eta_2, \alpha) e^{ik_\xi(\alpha)\xi} d\alpha \quad (4)$$

with $\Re k_\xi(\alpha) \geq 0$, $\Im k_\xi(\alpha) \geq 0$ and a bounded function $\mathbf{c}(\eta_1, \eta_2, \alpha)$. Hence \mathbf{E}_{sc} is a superposition of outgoing or evanescent waves in ξ direction. In our notation we have assumed that there exists a *global* (η_1, η_2, ξ) -coordinate system for the exterior domain. But in the following only the global meaning of the ξ coordinate as explained in Section 2 will be used, so η_1 and η_2 may also be considered as coordinates of a local chart for a subdomain of $\partial\Omega_{\text{int}}$. For $\gamma = 1 + i\sigma$ the complex continuation, $\xi \mapsto \gamma\xi$, $\mathbf{E}_{\text{sc},\gamma}(\cdot, \cdot, \xi) = \mathbf{E}_{\text{sc}}(\cdot, \cdot, \gamma\xi)$ gives

$$|\mathbf{E}_{\text{sc},\gamma}| \leq e^{-\kappa x_2} C, \quad (5)$$

with $\kappa = \min_\alpha \{\Im k(\alpha), \sigma \Re k(\alpha)\}$. Therefore $\mathbf{E}_{\text{sc},\gamma}(\cdot, \cdot, \xi)$ decays exponentially fast with growing generalized distance ξ to the coupling boundary. The idea is to restrict the complex continuation of the exterior domain problem to a truncated domain Ω_ρ and to impose a zero Neumann boundary condition at $\partial\Omega_\rho$. In the next section we will give a corresponding variational problem which can be discretized with the finite element method where we will use a tensor product ansatz in the truncated exterior domain Ω_ρ based on the triangulation of the

Algorithm 1 Adaptive PML method

Require: $\epsilon, \sigma, h_{\text{int}}, \kappa_{\text{min}}$

Compute $N_{\text{p.w}}$ and ξ_{max} depending on h_{int} and finite element order

while (not converged) **do**

$\xi_0 = 0.0; \xi_1 = h_{\text{int}}; N = 1;$

while $(-\ln(\epsilon)/(\xi_N \sigma) < \kappa_{\text{min}})$ **do**

$\xi_{N+1} = \xi_N + \max\{h_{\text{int}}, 2\pi\sigma\xi_N/(-\ln(\epsilon))/N_{\text{p.w}}\}.$

if $(\xi_{N+1} > 1/\epsilon)$ **then**

break

else

$N = N + 1$

end if

end while

Compute solution u with PML discretization $\{\xi_0, \xi_1, \dots, \xi_N\}$

if $\|u(\cdot, \xi_N)\| \leq \epsilon \|u(\cdot)\|$ **then**

converged

else if $\xi_N > \xi_{\text{max}}$ **then**

break

else

$\kappa_{\text{min}} = \kappa_{\text{min}}/2$

end if

end while

surface $\partial\Omega_{\text{int}}$ and a 1D mesh in ξ -direction, $\{0, \xi_1, \xi_2, \dots, \xi_N\}$. In this section we present an algorithm for the automatic determination of optimal discretization points ξ_j .

As can be seen from Equation (5) the PML method only effects the outgoing part with $\Re k_\xi$ strictly larger than zero. Field contributions with an large $\Re k_\xi$ component are efficiently damped out. Furthermore evanescent field contributions are damped out independently of the complex continuation. For a proper approximation of the oscillatory and exponential behavior a discretization that is fine enough is needed to resolve the field. In contrast to that anomalous modes or “near anomalous” modes with $k_\xi \sim 0$ enforce the usage of a large ρ but can be well approximated with a relatively coarse discretization in ξ . Such “near anomalous” modes typically occur in the periodic setting but may also be present for isolated structures with a layered exterior domain.¹¹ Hence for an efficient numerical approximation of the scattered field one must use an adaptive discretization. It is useful to think of the complex continuation as a high-frequency filter. With a growing distance ξ to the interior coupling boundary the higher frequency contributions are damped out so that the discretization can be coarsened.

For a given threshold ϵ we introduce the cut-off function

$$\kappa_{\text{co},\epsilon}(\xi) = -\ln(\epsilon)/\xi .$$

At $\xi' > 0$ each component in the expansion (4) with $\kappa > \kappa_{\text{co},\epsilon}(\xi')$ is damped out by a factor smaller than the threshold ϵ ,

$$e^{-\kappa\xi'} < e^{-\kappa_{\text{co},\epsilon}(\xi')\xi} = e^{\ln(\epsilon)} = \epsilon.$$

Assuming that this damping is sufficient we are allowed to select a discretization which must only approximate the lower frequency parts with $\kappa \leq \kappa_{\text{co},\epsilon}(\xi)$ for $\xi > \xi'$. If we use a fixed number $N_{\text{p.w}}$ of discretization points per (generalized) wavelength $2\pi/\kappa$ we get the following formula for the *a priori* determination of the local mesh width $h(\xi) = 2\pi\sigma/\kappa_{\text{co},\epsilon}(\xi)/N_{\text{p.w}}$. Since $\kappa_{\text{co},\epsilon}(\xi) \rightarrow \infty$ for $\xi \rightarrow 0$ the local mesh width is zero at $\xi = 0$. As it is not reasonable to use a finer discretization in the exterior domain than in the interior domain we bound the local mesh width by the minimum mesh width h_{int} of the interior domain discretization on the coupling boundary,

$$h(\xi) = \max\{h_{\text{int}}, 2\pi\sigma/\kappa_{\text{co},\epsilon}(\xi)/N_{\text{p.w}}\}.$$

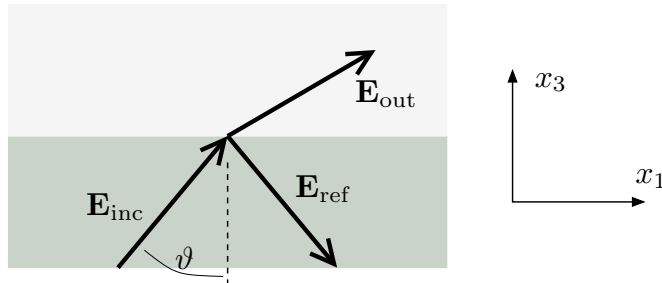


Figure 2. Test problem for adaptive PML discretization. A plane wave is incident under an angle ϑ from the lower material with refractive index $n_{\text{sub}} = 1.5$. The upper material consists of air ($n_{\text{sup}} = 1.0$). According to Snell's law the field is totally reflected for an incident angle greater or equal to the *critical angle* $\vartheta_c = 180 \cdot \text{asin}(1.0/1.5)/\pi \approx 41.81$.

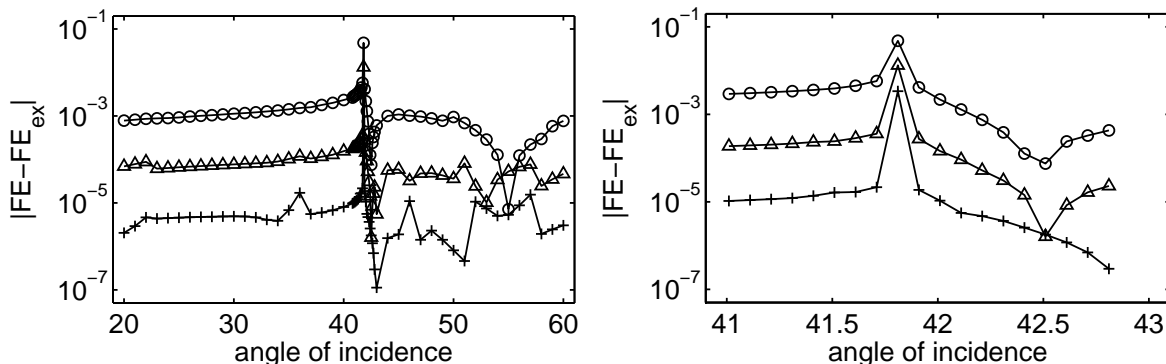


Figure 3. Left: Field energy error in the interior domain. The three data sets (\circ , \triangle , $+$) correspond to different refinement levels of the interior domain. Right: Zoom into the left figure near the critical angle.

The parameters ϵ and $N_{\text{p,w}}$ are also fixed accordingly to the interior domain discretization quality. The grid $\{\xi_0, \xi_1, \xi_2, \dots\}$ is recursively constructed by

$$\xi_{n+1} = \xi_n + h(\xi_n).$$

This way ξ_n grows exponentially with n . To truncate the grid we assume that components in the expansion with $\kappa < \kappa_{\text{min}}$ can be neglected so that the grid $\{\xi_0, \xi_1, \dots, \xi_N\}$ is determined by $\kappa_{\text{co},\epsilon}(\xi_N) < \kappa_{\text{min}} \leq \kappa_{\text{co},\epsilon}(\xi_{N-1})$. As an *a posteriori* control we check if the field is indeed sufficiently damped out at ξ_N , $\|u(\cdot, \xi_N)\| \leq \epsilon \|u(\cdot)\|$. Otherwise we recompute the solution with $\kappa_{\text{min}} \rightarrow \kappa_{\text{min}}/2^*$. Since for an anomalous mode the field is not damped at all we restrict the maximum ξ_N to $\xi_N < \pi/k_0/\epsilon$. The pseudocode to the algorithm is given in Algorithm 1.

To demonstrate the performance of the adaptive PML algorithm we compute the reflection of a plane wave at a material interface, cf. Figure 2. In x_1 -direction we use Bloch periodic boundary conditions.¹² We vary the angle of incidence from $\vartheta = 20^\circ$ to $\vartheta = 60^\circ$. Further the incoming field is rotated along the x_3 axis by an angle of 45° , so that the incidence is twofold oblique (conical). Hence the unit direction of the incoming field is equal to $\hat{k} = (\cos 45^\circ \sin \vartheta, \cos \vartheta, \sin 45^\circ \sin \vartheta)$. We use an interior domain of size 1.5×1 in wavelength scales. To measure the error we compute the field energy within the interior domain and compare it to the analytic value. In Figure 3 the error is plotted for different refinement levels of the interior domain. The “+” line corresponds to the finest level. In Figure 4 the automatically adapted thickness of the PML is plotted (left) and the number of discretization points N in ξ direction (right). As expected a huge layer is constructed automatically at the critical angle, whereas the total number of discretization points remains moderate. As can be seen in Figure 3

*This strategy proved useful in many experiments. However we consider to refine it.

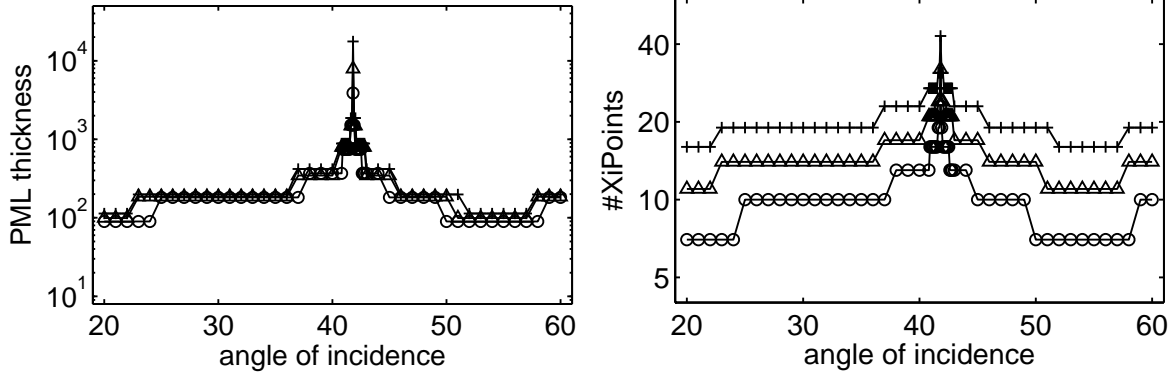


Figure 4. Left: Thickness of the PML layer in unit lengths. At the critical angle the thickness is up to 10^4 times larger than the size of the interior domain. Right: Number of discretization points ξ_j used in the radial direction (x_2). Although the required thickness of the layer is huge the number of unknowns used in the PML layer remains moderate.

Step	ΔE	$\Delta E'$
0	0.359850	0.335129
1	0.159358	0.166207
2	0.048779	0.049502
3	0.012911	0.012912
4	0.003274	0.003266
5	0.000205	0.000820
6	0.000206	0.000205
7	0.000051	0.000051

Table 1. Convergence of field energy at the critical angle of incidence. The first column corresponds to the interior mesh refinement step. The relative error of the electric field energy in the interior domain is given in the second column, $\Delta E = \frac{|\|\mathbf{E}_{ex}\|_{L^2}^2 - \|\mathbf{E}_h\|_{L^2}^2|}{\|\mathbf{E}_{ex}\|_{L^2}^2}$. The third column displays the relative error of the magnetic field energy $\Delta E' = \frac{|\|\text{curl } \mathbf{E}_{ex}\|_{L^2}^2 - \|\text{curl } \mathbf{E}_h\|_{L^2}^2|}{\|\text{curl } \mathbf{E}_{ex}\|_{L^2}^2}$ is given. For fixed PML thickness the solution converges towards the analytical result as the interior mesh is refined.

the maximum error appears at the critical angle. From that one may suspect a failure of the automatic PML adaption. But a closer analysis reveals that the chosen discretization in the PML layer is sufficient as can be seen from Table 1. Here the thickness of the perfectly matched layer has been fixed and we further refined the interior domain. By this means we observe convergence to the true solution but the convergence rate is halved at the critical angle. Hence the maximum error at the critical angle is caused by an insufficient interior discretization. We conjecture that this is due to a dispersion effect. Since near the critical angle the wave \mathbf{E}_{out} is traveling mainly along the x_1 - direction it reenters the periodic domain, leading to large “path length”.

5. VARIATIONAL FORMULATION

So far the overall scattering problem was given as an interior domain problem coupled to an exterior domain problem via boundary matching conditions. In this section we give (without proof) a variational problem in $H(\text{curl}, \Omega \cup \Omega_{\text{ext}})$ for the computation of the composed field $\tilde{\mathbf{E}}$ with $\tilde{\mathbf{E}} = \mathbf{E}_{\text{int}}$ in Ω_{int} and $\tilde{\mathbf{E}} = \mathbf{E}_{\text{sc}, \gamma} + \Pi(\mathbf{E}_{\text{inc}} \times \vec{n})$ in Ω_{ext} . Details for the 2D case are given in our paper.¹³ Here Π is the extension operator defined as $\Pi(\mathbf{E}_{\text{inc}} \times \vec{n}) = \chi_{[0, \epsilon)}(1 - \xi/\epsilon)(\mathbf{E}_{\text{inc}} \times \vec{n})$.

For each face F of the transparent boundary $J_F(\eta_1, \eta_2, \xi)$ denotes the Jacobian of the mapping $Q_F(\eta_1, \eta_2, \xi)$. Further we introduce the *pulled back* field $\mathbf{u}_*(\eta_1, \eta_2, \xi) = J^t \mathbf{u}(Q_F(\eta_1, \eta_2, \xi))$ for any field defined on Ω_{ext} . With the definition

$$\text{curl}_\gamma = (\partial_{\eta_2} - \frac{1}{\gamma} \partial_\xi, -\partial_{\eta_1} + \frac{1}{\gamma} \partial_\xi, \partial_{\eta_1} - \partial_{\eta_2})$$

and the transformed tensors $\mu_* = |J|J^{-1}\mu J^{-t}$ and $\varepsilon_* = |J|J^{-1}\varepsilon J^{-t}$ the composed field $\tilde{\mathbf{E}}$ satisfies

$$\begin{aligned} & \int_{\Omega_{\text{int}}} \text{curl } \Psi \mu^{-1} \text{curl } \tilde{\mathbf{E}} - \omega^2 \Psi \varepsilon \tilde{\mathbf{E}} + \gamma \sum_F \int_{P_u} \text{curl}_\gamma \Psi_* \mu_*^{-1} \text{curl}_\gamma \tilde{\mathbf{E}}_* - \omega^2 \Psi_* \varepsilon_* \tilde{\mathbf{E}}_* = \\ & - \int_{\partial\Omega_{\text{int}}} \Phi \cdot \mu^{-1} \text{curl}_3 \mathbf{E}_{\text{inc}} \times \vec{n} + \gamma \sum_F \int_{P_u} \text{curl}_\gamma \Psi_* \mu_*^{-1} \text{curl}_\gamma \Pi(\mathbf{E}_{\text{inc}} \times \vec{n}) - \omega^2 \Psi_* \varepsilon \Pi(\mathbf{E}_{\text{inc}} \times \vec{n}). \end{aligned}$$

Although this equation looks complicated it can be easily discretized with finite elements. In fact the terms in the sum over the faces F are already given in unit coordinates of the prism. So it is advantageous to use a prismatic mesh in the exterior domain. This way we fix the *global* discretization points $\{\xi_0 = 0, \xi_1, \dots, \xi_N\}$ as described in the previous section and split the truncated exterior domain Ω_{ξ_N} into the prisms $Q_F(P_{\xi_{i+1}} \setminus P_{\xi_i})$ with $i < N$. In the interior domain we use a tetrahedral mesh which we fit non-overlapping to the exterior domain mesh. Introducing the bilinear forms

$$\begin{aligned} a_{\text{int}}(\Psi, \Phi) &= \int_{\Omega_{\text{int}}} \text{curl } \Psi \mu^{-1} \text{curl } \tilde{\mathbf{E}} \\ b_{\text{int}}(\Psi, \Phi) &= \int_{\Omega_{\text{int}}} \Psi \varepsilon \tilde{\mathbf{E}} \\ a_\gamma(\Psi, \Phi) &= \gamma \sum_F \int_{P_\rho} \text{curl}_\gamma \Psi_* \mu_*^{-1} \text{curl}_\gamma \tilde{\mathbf{E}}_* \\ b_\gamma(\Psi, \Phi) &= \gamma \sum_F \int_{P_\rho} \Psi_* \varepsilon_* \tilde{\mathbf{E}}_* \\ a(\Psi, \Phi) &= a_{\text{int}}(\Psi, \Phi) + a_\gamma(\Psi, \Phi) \\ b(\Psi, \Phi) &= b_{\text{int}}(\Psi, \Phi) + b_\gamma(\Psi, \Phi) \end{aligned}$$

and

$$g(\Psi) = - \int_{\partial\Omega_{\text{int}}} \Phi \cdot \mu^{-1} \text{curl}_3 \mathbf{E}_{\text{inc}} \times \vec{n}$$

the variational problem truncated to $\Omega_{\text{int}} \cup \Omega_\rho$ can be casted to

$$a(\Psi, \tilde{\mathbf{E}}) - \omega^2 b(\Psi, \tilde{\mathbf{E}}) = g(\Psi) + a_\gamma(\Psi, \Pi(\mathbf{E}_{\text{inc}} \times \vec{n})) - \omega^2 b_\gamma(\Psi, \Pi(\mathbf{E}_{\text{inc}} \times \vec{n}))$$

for all $\Psi \in H(\text{curl}, \Omega_{\text{int}} \cup \Omega_{\rho})$. To discretize this variational problem we use Nedelec's vectorial finite elements¹⁴ with local ansatz functions $\{\mathbf{v}_1, \mathbf{v}_2, \dots, \mathbf{v}_n\}$. Making the ansatz $\tilde{\mathbf{E}} = \sum u_i \mathbf{v}_i$ this yields the algebraic system

$$(A - \omega^2)Bu = f$$

with $f_i = g(\mathbf{v}_i) + a_{\gamma}(\mathbf{v}_i, \Pi(\mathbf{E}_{\text{inc}} \times \vec{n})) - \omega^2 b_{\gamma}(\mathbf{v}_i, \Pi(\mathbf{E}_{\text{inc}} \times \vec{n}))$, $A_{i,j} = a(\mathbf{v}_i, \mathbf{v}_j)$ and $B_{i,j}$ accordingly.

6. TIME DOMAIN PRECONDITIONER

In this section we propose a novel preconditioner for the algebraic system

$$(A - \omega^2 B)u = f \tag{6}$$

derived in the last section. Since $\omega^2 > 0$ this system is indefinite. Hence standard multigrid methods will suffer from slow convergence rates or may even not converge. Other numerical methods like the Finite Difference Time Domain method do not start from the time-harmonic Maxwell's equations. Instead they simulate temporal transient effects. For practical purposes the computation time is prohibitively large until the steady state is reached.¹⁵ Even worse, the usage of an explicite time stepping scheme forces the usage of very small time steps to avoid instabilities.

Here we propose a preconditioner for the time-harmonic system which makes use of the fact that the solution we want to compute is the steady state solution to a transient process. This is the reason why we call this preconditioner "time domain" preconditioner. Instead of using time dependent Maxwell's equations one may use another dynamical system whose steady state solution is the field in mind. For example the above solution u is the steady state solution to the time dependent problem

$$i \frac{d}{dt} Bu(t) = Au(t) - f e^{-i\omega^2 t}$$

which looks like the time dependent Schrödinger equation. But we may also start from a time discrete system, such as

$$i \frac{1}{\tau} (Bu_{n+1} - Bu_n) = Au_{n+1} - p^{n+1} f \tag{7}$$

with $p = (\frac{1}{1+i\omega^2\tau})$ corresponding to a time discretization of the above Schrödinger like equation with the implicate Euler method. One proves that if the original system has a steady state solution then the sequence $\{u_0, p^{-1}u_1, p^{-2}u_2, \dots\}$ converges to the solution u of Equation (6) indepently of the selected time step τ . In our code we typically fix $\tau = 0.1/\omega^2$. Starting from a randomized initial guess u_0 we compute a fixed number N of iterations to the recursion formula (7) which yields the sequence $\{u_0, p^{-1}u_1, \dots, p^{-N}u_N\}$. In each iteration step the arising system is solved by an multigrid method up to a moderate accuracy. We then compute the minimum residual solution within the space spanned by the last $M < N$ vectors in this sequence. The so constructed approximate solver is used as a preconditioner for a standard iterative method for indefinite problems such as GMRES or BCGSTAB.¹⁶

Other discrete schemes may be used to improve the convergence to the steady state solution. For example it is promising to use schemes stemming from higher order Runge-Kutta methods or multi-step methods for the discretization of the original wave equation or the Schrödinger like equation above.

7. RESONANCE PROBLEMS

A resonance is a purely outgoing field which satisfies the time harmonic Maxwell's equation for a certain $\omega \in \mathbb{C}$. We again assume that an expansion as in Equation (4) is valid but we must drop the assumption $\Im k_{\xi}(\alpha) \geq 0$. Hence a resonance mode may exponentially grow with the generalized distance ξ . In this case we must choose σ large enough in the PML method to achieve an exponential damping of the complex continued solution. Using a finite element discretization as in the previous section we end up with the algebraic eigenvalue problem

$$Au = \omega^2 Bu. \tag{8}$$

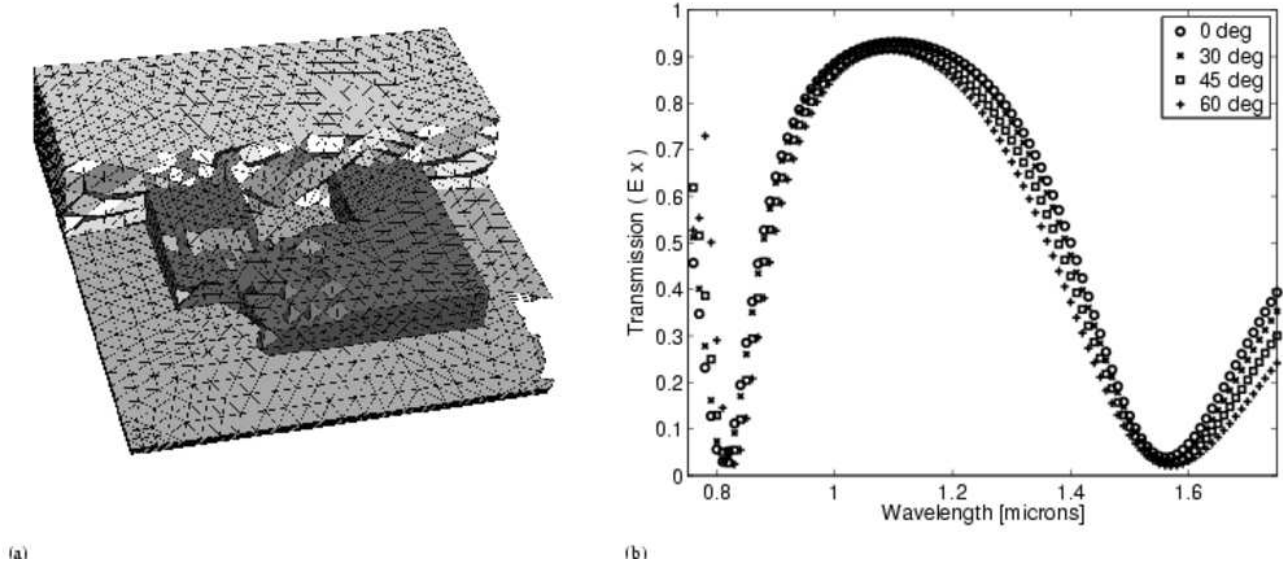


Figure 5. (a) Visualization of a part of the tetrahedra of the spatial discretization of the interior SRR geometry. Dark gray tetrahedra: gold SRR; light gray: air; gray: ITO. Periodic boundary conditions apply at the right/left and front/back. Prism elements discretizing the exterior domain (on the top/bottom) are not shown. (b) Transmission spectra of light fields incident onto an SRR for different angles of incidence (For details see also¹⁷). The transmission minimum at $\lambda \sim 1.5\mu\text{m}$ is due to the excitation of the fundamental resonance of the SRRs. (See original publication for images with higher resolution.)

8. META-MATERIALS: SPLIT RING RESONATORS

Split-ring resonators (SRR's) can be understood as small LC circuits consisting of an inductance L and a capacitance C . The circuit can be driven by applying external electromagnetic fields. Near the resonance frequency of the LC -oscillator the induced current can lead to a magnetic field opposing the external magnetic field. When the SRR's are small enough and closely packed – such that the system can be described as an effective medium – the induced opposing magnetic field corresponds to an effective negative permeability, $\mu < 0$, of the medium.

Arrays of gold SRR's with resonances in the NIR and in the optical regime can be experimentally realized using electron-beam lithography, where typical dimensions are one order of magnitude smaller than NIR wavelengths. Details on the production can be found in Linden and Enkrich.^{1,2}

Due to the small dimensions of the LC circuits their resonances are in the NIR and optical regime.² Figure 5(a) shows the tetrahedral discretization of the interior domain of the geometry. Figure 5(b) shows results from FEM simulations of light scattering off a periodic array of SRR's for different angles of the incident light.¹⁷ At $\lambda \sim 1.5\mu\text{m}$ the transmission is strongly reduced due to the excitation of a resonance of the array of SRR's. This excitation occurs for all investigated angles of incidence.

When one is interested to learn about resonances, obviously it is rather indirect and time-consuming to calculate the scattering response of some incident light field and then to conclude the properties of the resonance. We have therefore also directly computed resonances of SRR's by solving Eqn. (8). Special care has to be taken in constructing appropriate PML layers, as in this case the previously described adaptive strategy for the PML is more involved. We have therefore set these parameters by hand. We have computed the fundamental resonance with $\omega = 1.302023 \cdot 10^{15} - 0.399851 \cdot 10^{15}i$.

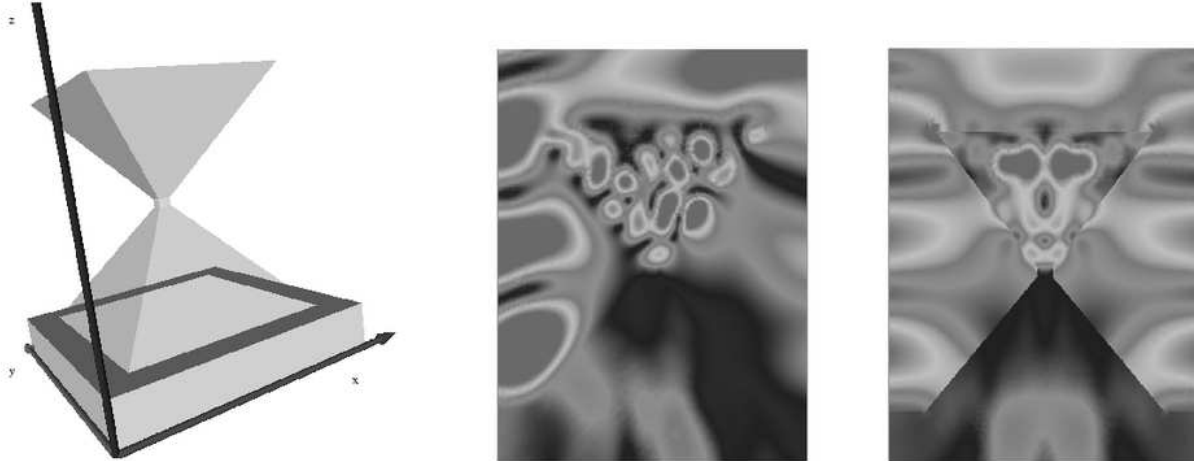


Figure 6. Pyramidal nano resonator. The structure is mounted on a Gallium Arsenid (GaAs) substrate. The middle figure shows the field amplitude in the x - z plane. The right figure shows the field amplitude in the y - z plane. (See original publication for images with higher resolution.)

9. PYRAMIDAL NANO-RESONATOR

This type of nano resonators is proposed to be used as optical element in quantum information processing.¹⁸ The structure is as depicted in Figure 6 (left). We have simulated the illumination of the structure with a plane wave of a vacuum wavelength $\lambda_0 = 1.55\mu\text{m}$ and a unit direction $\hat{k} = (\sqrt{0.5}, 0, -\sqrt{0.5})$. The incident field was polarized in x -direction. Figure 6 shows the field amplitude in the computational domain. More than five million of unknowns were used in the discretization. With the preconditioner proposed in Section 6 ($N=20$) the GMRES method exhibited a convergence rate of 0.8.

ACKNOWLEDGMENTS

We thank R. Klose, A. Schädle, P. Deuffhard and R. März for fruitful discussions, and we acknowledge support by the initiative DFG Research Center *Matheon* of the Deutsche Forschungsgemeinschaft, DFG, and by the DFG under contract no. BU-1859/1.

REFERENCES

1. S. Linden, C. Enkrich, M. Wegener, C. Zhou, T. Koschny, and C. Soukoulis, “Magnetic response of metamaterials at 100 Terahertz,” *Science* **306**, p. 1351, 2004.
2. C. Enkrich, M. Wegener, S. Linden, S. Burger, L. Zschiedrich, F. Schmidt, C. Zhou, T. Koschny, and C. M. Soukoulis, “Magnetic metamaterials at telecommunication and visible frequencies,” *Phys. Rev. Lett.* **95**, p. 203901, 2005.
3. V. G. Veselago, “The electrodynamics of substances with simultaneously negative values of ϵ and μ ,” *Sov. Phys. Usp.* **10**, p. 509, 1968.
4. J. B. Pendry, “Negative refraction makes a perfect lens,” *Phys. Rev. Lett.* **85**, p. 3966, 2000.
5. J.-P. Bérenger, “A perfectly matched layer for the absorption of electromagnetic waves,” *J. Comput. Phys.* **114**(2), pp. 185–200, 1994.
6. F. Schmidt, “A New Approach to Coupled Interior-Exterior Helmholtz-Type Problems: Theory and Algorithms,” 2002. Habilitation thesis, Freie Universität Berlin.
7. M. Lassas and E. Somersalo, “On the existence and convergence of the solution of PML equations.,” *Computing No.3, 229-241* **60**(3), pp. 229–241, 1998.

8. M. Lassas and E. Somersalo, "Analysis of the PML equations in general convex geometry," in *Proc. Roy. Soc. Edinburgh Sect. A* 131, (5), pp. 1183–1207, 2001.
9. T. Hohage, F. Schmidt, and L. Zschiedrich, "Solving time-harmonic scattering problems based on the pole condition: Convergence of the PML method," Tech. Rep. ZR-01-23, Konrad-Zuse-Zentrum (ZIB), 2001.
10. A. Schädle, L. Zschiedrich, S. Burger, R. Klose, and F. Schmidt, "Domain Decomposition Method for Maxwell's Equations: Scattering off Periodic Structures," *in preparation*, 2006.
11. R. Petit, *Electromagnetic Theory of Gratings*, Springer-Verlag, 1980.
12. S. Burger, R. Klose, A. Schädle, F. Schmidt, and L. Zschiedrich, "FEM modelling of 3d photonic crystals and photonic crystal waveguides," in *Integrated Optics: Devices, Materials, and Technologies IX*, Y. Sidorin and C. A. Wächter, eds., **5728**, pp. 164–173, Proc. SPIE, 2005.
13. L. Zschiedrich, R. Klose, A. Schädle, and F. Schmidt, "A new finite element realization of the Perfectly Matched Layer Method for Helmholtz scattering problems on polygonal domains in 2D," *J. Comput Appl. Math.*, 2005. in print; published online.
14. P. Monk, *Finite Element Methods for Maxwell's Equations*, Clarendon Press, Oxford, 2003.
15. S. Burger, R. Köhle, L. Zschiedrich, W. Gao, F. Schmidt, R. Mrz, and C. Nölscher, "Benchmark of FEM, Waveguide and FDTD Algorithms for Rigorous Mask Simulation," in *Photomask Technology*, J. T. Weed and P. M. Martin, eds., **5992**, pp. 368–379, SPIE.
16. R. Freund, G. Golub, and N. Nachtigal, "Iterative solution of linear systems," *Acta Numerica*, 1992.
17. S. Burger, L. Zschiedrich, R. Klose, A. Schädle, F. Schmidt, C. Enkrich, S. Linden, M. Wegener, and C. M. Soukoulis, "Numerical investigation of light scattering off split-ring resonators," in *Metamaterials*, T. Szoplik, E. Özbay, C. M. Soukoulis, and N. I. Zheludev, eds., **5955**, pp. 18–26, Proc. SPIE, 2005.
18. H. K. W. Löffler, "private communication, CFN Karlsruhe," 2005.